JOURNAL OF THERMOPHYSICS AND HEAT TRANSFER
Vol. 24, No. 1, January–March 2010

Mixed-Convection Heat Transfer from Simulated Air-Cooled Electronic Devices: Experimental and Numerical Study

Meftah Hrairi,* Mirghani Ishaq Ahmed,† and Ahmad Faris Ismail†
International Islamic University Malaysia, 50728 Kuala Lumpur, Malaysia

DOI: 10.2514/1.44154

Air-cooling characteristics of an electronic-device heat sink have been experimentally and numerically investigated under various operating conditions for air. Flowing air velocities of 0–7.1 m/s were circulated through a wind tunnel with a rectangular section. The lower surface of the wind tunnel was equipped with 5 by 3 heat sources subjected to uniform heat flux. From the experimental measurements, surface temperature distributions of the discrete heat sources were obtained and effects of Reynolds numbers on these temperatures were investigated. A computational fluid dynamics analysis of the cooling process was conducted to simulate the system and to calculate the required cooling rate. A relation was identified between the thermal-wake function and capability of the software to give better estimations of the circuit-board temperatures. Overall, the obtained results showed good agreement between the simulation and the experimental results. In particular, it was found that surface temperatures of heated modules decrease with increasing Reynolds number.

Nomenclature

A	=	area, m^2
C_p	=	specific heat, kJ/kg K
Gr_L	=	Grashof number, $[g\beta(T_{ac} - T_{air})L^3]/\nu_{air}^2$
g	=	gravitational acceleration, m/s^2
h	=	specific enthalpy, kJ/kg
$\hbar$	=	pressure head, m
h^*	=	coefficient of heat convection, kW/m^2 K
k	=	thermal conductivity, W/m K
L	=	length of a single electronic module, mm
Nu_L	=	Nusselt number, hL/k_{air}, $qL/[A_s(T_{ac} - T_{ref})k_{air}]$
Pr	=	Prandtl number, $C_{p,air}\mu_{air}/k_{air}$
Q_{cond}	=	amount of heat loss by conduction, kJ
Q_{conv}	=	amount of heat convected by air, kJ
Q_{rad}	=	amount of heat loss by radiation, kJ
Q_{tot}	=	total heat generated by the chip, kJ
q	=	convective heat flux, kW
Re_L	=	Reynolds number, $\nu_{in}L/\nu_{air}$
Ri	=	Richardson number, Gr/Re^2
S	=	heat generation term, kJ
T_{ac}	=	modules actual temperature, K
$T_{b,bot}$	=	bottom of the board temperature, K
$T_{b,top}$	=	top of the board temperature, K
T_i	=	modules initial temperature, K
T_{ref}	=	reference temperature, K
t_b	=	thickness of the board, mm
V	=	volume, m^3
v	=	velocity, m/s
β	=	thermal expansion coefficient, 1/K
Γ	=	species concentration, kg/kg
θ_i	=	thermal-wake function
μ	=	dynamic viscosity, kg/m s
ν	=	kinematic viscosity, m^2/s
ρ	=	density, kg/m^3
ϕ	=	general field parameter

Received 10 March 2009; revision received 17 August 2009; accepted for publication 3 October 2009.

*Assistant Professor, Department of Mechanical Engineering, P.O. Box 10.
†Professor, Department of Mechanical Engineering, P.O. Box 10.

I. Introduction

DEMAND for electronic products requires smaller packages with higher performance and more functions than the preceding generation. The increased thermal performance required of these smaller parts is mandatory for producing high-efficiency reduced-size systems. As the reliability of the electronic components is directly related to the temperature [1], appropriate cooling designs are required in order to remove the heat from the components and maintain their temperature under required safety limits [2–4]. The cooling of electronic systems can be accomplished by continuously removing heat from them at an adequate rate. Failure to do so may allow the generated heat to cause burning or overheating problems that lead to system failure and costly damage.

Many techniques are used for cooling the electronic circuits. Most embedded systems today use either heat sinks and fans, air cooling, or conduction cooling. However, some leading-edge applications use flow-through liquid cooling or spray cooling. Among these various cooling techniques for electronic parts, air-cooled forced-convection cooling remains the most used technique, as it has the advantages of convenience, simple design, easy maintenance, high reliability, and low costs [5–7].

To cope with the increased cooling requirement, several theoretical and experimental studies have been carried out to improve the heat removal rate of forced-convective cooling with air by using heat sinks with different shapes, materials, flow patterns, etc. [8]. These studies are based on the fluid flow around obstacles mounted on a wall base, on which the phenomenon of mixed convection is observed around the localized heat sources. Bar-Cohen [9] resolved the cooling problem of electronic modules by means of heat transfer, carried out some studies on the cooling of chip packages [10], and introduced a compact model for chip packages [11]. Heat transfer and flow characteristics of four heat-source locations were studied in [12]. Studies by Kang et al. [13] found that heat transfer can be improved significantly by buoyancy-driven secondary flow. However, the effect of thermal-wake generation was not fully understood because of the use of a single heat source. Numerical study of the unsteady and transitional characteristics of mixed convection of airflow in a channel was conducted in [14]. The significant effect of the thermal boundary flow pattern on the secondary flow pattern and on the heat flow distribution over the surface was also shown [15]. Experimental investigations have been carried out to study the effects of the varying duct dimensions and obstruction dimensions on the convection from the surface of the heat-generating obstructions to the airflow [16], the effects of using ribs to enhance the convective heat transfer [17], and the optimum spacing problem in mixed convection

[18]. A modified 5% deviation rule to define the natural-, mixed-, and forced-convection regimes was proposed by Choi and Kim [19].

In most of the previous work, the impact of the transitional characteristics of mixed convection on the accuracy of the numerically predicted results has not been investigated. The thermal-wake generation and the actual effect of buoyancy-driven secondary flow have not been studied thoroughly.

This study presents a numerical analysis of the air cooling of a simulated electronic board using computational fluid dynamics (CFD) along with an experimental work to validate the computed results. In particular, this paper will focus on the accuracy of the CFD results and on how the flow regime and the local thermal conditions affect them. It also assesses the importance of various parameters (axial position, Reynolds number, and wake function), since the underlying effects are still not well understood. The conjugate nature of the problem, due to coupling between convection in the fluid and conduction in the sources, is considered in the interpretation of the results. Correlating equations are obtained to predict heat transfer rates and the thermal-wake-generation function factor for different circumstances. Furthermore, an error analysis on the numerical results has been carried out.

II. Experimental Apparatus and Procedure

A. Experimental Setup

Figure 1 shows the schematic diagram of the experimental apparatus used in this study for the measurement of heat transfer characteristics for the simulated heat sink. The experimental apparatus is made of a wind tunnel with a rectangular section with electronic components mounted on a circuit board (Fig. 1a). The setup consists of the test rig, a dc power supply for the electronic modules, a brushless blower, and a number of digital thermocouples. Electric heating elements (resistors) were embedded inside the obstructions that resemble the electronic components, and sets of thermocouples were used to read the surface temperature of the components (Fig. 1b). The test rig is divided into eight zones of airflow impedance. The zones are numbered sequentially, following the direction of airflow (Fig. 1c). Each zone will be analyzed individually for cross-sectional area changes and heat loss. The details of zone 5, which contains the simulated electronic board, is shown in Fig. 1d.

Thermocouples were placed on different modules to measure their surface temperatures. A vane anemometer was placed at the exit of the blower to measure the air velocity for every set of applied fan speeds. The system usually takes about 1 h and 30 min to reach a steady state. Natural-convection heat transfer measurements were taken while the fan was kept off. Heaters were put on, and enough time was allowed for the system to reach a steady-state condition. When the steady-state condition was achieved (by checking that module temperature does not change with time), the local temperatures of the modules were recorded. A similar procedure was then followed for the forced-convection heat transfer measurements. In this part of the test, the fan speed was set at different values. When a steady-state condition was achieved at each value of fan speed, the temperature measurements of the modules were recorded.

B. Handling of Experimental Data

During all of the experiments, it was noted that the heat dissipation from each of the discrete heat sources was very similar within one row. Consequently, experimental data were reduced in terms of row-average values for each heater row. The local heat transfer coefficient for a row was calculated by dividing the heat flux supplied to each chip by the temperature difference between the surface temperature of the chip and the fluid temperature just below the chip, as shown in the following equation:

$$h = \frac{q}{A_s(T_{ac} - T_{ref})} \tag{1}$$

The reference temperature represents the local air temperature above the modules. It is calculated by using an approximated air-temperature formulation:

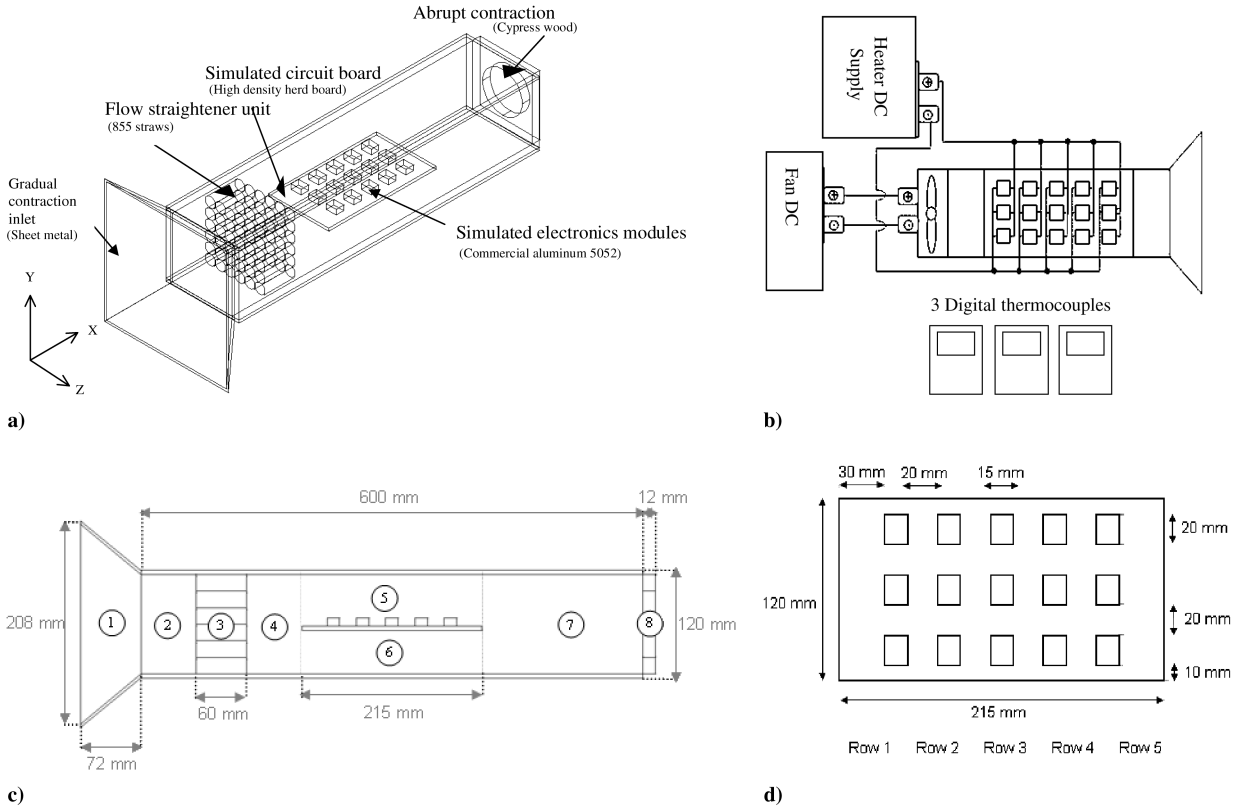

Fig. 1 Schematic diagram of the experimental setup: a) rectangular section of wind tunnel, b) experimental apparatus assembly, c) zones of airflow impedance, and d) heat-source layout.

$$T_{\text{ref}} = \left(\frac{T_{\text{in}} + T_{\text{ac}}}{2} + T_i\right) \Big/ 2 \tag{2}$$

The temperature of the rows closer to the air exit is affected by the thermal-wake phenomenon. The thermal wake happens when heat-generating components are placed along the flow stream direction. This function is defined as

$$\theta_i = \frac{T_i - T_{\text{ref}}}{T_{\text{ac}} - T_{\text{ref}}} \tag{3}$$

The volumetric maximum flow rate was found to be 11.8×10^{-3} m^3/s. This is the maximum flow rate of the fan that is used in the test rig.

The maximum Reynolds number based on the module length is 1418, which should mean laminar flow. Buoyancy forces are very important in mixed-convection flow. The heat induced buoyancy effects are expressed by the Grashof number, and the relative importance of the forced and buoyant effects is indicated by the Richardson number. With the increasing Richardson number, the heat transfer process around the heated source changes from forced-convection to a mixed-convection regime.

C. Heat Loss Analysis

At steady-state conditions, heat convection is found by considering the balance of the heat generated by the chips, the heat conducted through the board, and the heat radiated to the surroundings. Equation (4) shows the heat balance for a steady-state condition:

$$Q_{\text{conv}} = Q_{\text{tot}} - Q_{\text{cond}} - Q_{\text{rad}} \tag{4}$$

The radiation loss for each module was estimated to 2% of the input power of 1.96 W. However, the local heat conducted through the board, calculated using Eq. (5), was found to vary from 0.134 to 0.781 W, depending on fan velocity and the heat-source location:

$$Q_{\text{cond}} = \frac{k_b A_{\text{eff}}}{t_b}(T_{b,\text{top}} - T_{b,\text{bot}}) \tag{5}$$

Therefore, the largest amount of heat is lost from the circuit board by convection (from 1.167 to 1.826 W, depending on fan velocity and the heat-source location).

D. Uncertainty Analysis

An uncertainty analysis was performed to evaluate the accuracy of the data in this study. This analysis was conducted on all measured quantities as well as the quantities calculated using the measurement results. The uncertainty u_F, of the dependent variable F as a function of the uncertainties u_{xi}. associated with the independent variables x_i, is estimated according to the procedure reported in the literature [20–22], and this is given by the relation

$$u_F = \pm\left\{\sum_{i=1}^{n}\left[\left(\frac{\partial F}{\partial x_i}\right)^2 u_{x_i}^2\right]\right\}^{1/2} \tag{6}$$

Following this procedure, the uncertainty in the Reynolds number was evaluated to be around $\pm 4.1\%$. Uncertainty in the Nusselt number is around $\pm 5.4\%$ and in the Grashof number it is around $\pm 5\%$, which is primarily due to uncertainties in the convective heat flux values.

III. Numerical Approach

A. Numerical Solution Procedure

The CFD numerical process can solve the heat- and fluid-related governing equations. Furthermore, the fluid flow, heat transfer, and mass transfer could be determined through this simulation. One of the CFD schemes, finite volume method (FVM), is widely used in the computational fluid dynamics field. In the FVM, the domain is discretized into a finite set of control volumes or cells. The general conservation (transport) equation for mass, momentum, energy, etc., are discretized into algebraic equations and are treated in balance form for finite-sized control volumes. The CFD simulation is done by FLUENT, which is FVM-based CFD software. The general conservation equation is expressed by

$$\underbrace{\frac{\partial}{\partial t}\int_V \rho\phi \,\mathrm{d}V}_{\text{unsteady}} + \underbrace{\oint_A \rho\phi V \cdot \mathrm{d}A}_{\text{convection}} = \underbrace{\oint_A \Gamma\nabla\phi \cdot \mathrm{d}A}_{\text{diffusion}} + \underbrace{\int_V S_\phi \,\mathrm{d}V}_{\text{generation}} \tag{7}$$

Using this strategy, 2-D and 3-D models were first created in GAMBIT software. The appropriate boundary conditions were applied for each model before being exported to FLUENT solver. The segregated solver was selected for both cases. The option to solve the energy equation was enabled. The property of the air was set to the default values specified by the software. Properties of aluminum modules and the hard board were set according to the values used for heat transfer analysis. Because of the low velocities involved, this problem has been considered as an incompressible flow.

B. Grid Sensitivity and Convergence

A grid size study was conducted to determine the effects of grid resolution on the computational results and to finalize the grid structure to be used for the analysis. In this work, a grid of 36,467 elements is used on the finest level with denser, uniform grid spacing on the heating module and nonuniform grids elsewhere. The nonuniform grids have denser clustering near the module and the wall boundaries. A finer grid of 185,215 elements was also tested to check if variance in the grid spacing could increase the accuracy of the calculations. It was found that the refinement of the grid slightly improved the solution accuracy of the modules temperature, leading to a maximum relative difference of 4.4%. This comparison indicates that the coarse grid provides sufficient resolution and accuracy with less computational time, and hence this grid size was used for rest of the computations. Convergence was achieved when normalized residual values of continuity, velocities, and energy attained 4×10^{-3}, 1×10^{-3}, and 1×10^{-6}, respectively (Fig. 2).

IV. Results and Discussion

A. Measured Heat Transfer Coefficient

Figure 3 shows local heat transfer coefficients with respect to the row number for different Reynolds numbers. The local heat transfer coefficients seem to reach a uniform value approximately after the fourth row. This means that the fully developed thermal condition was reached after the fourth row. This pattern is in a very good agreement with Choi and Cho [23], who experimentally found that the local heat transfer coefficients reached a uniform value approximately after the fourth row (located at a distance of seven times the chip length), regardless of coolants and aspect ratios. Through his computational and experimental results, Anderson [24] also observed the attainment of fully developed conditions after the fourth row.

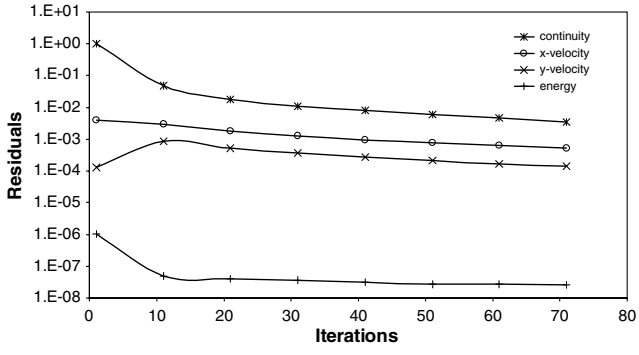

Fig. 2 Convergence histories for the governing equations.

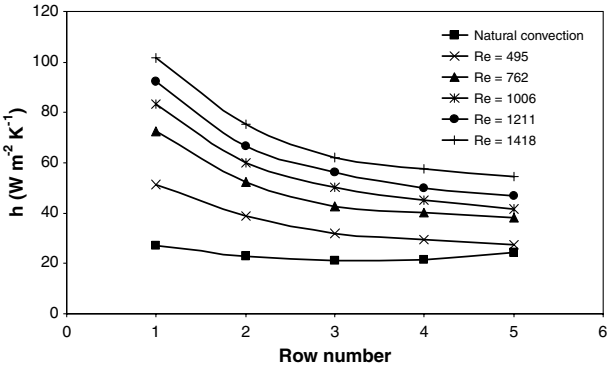

Fig. 3 Local heat transfer coefficients with respect to row number for different values of Reynolds number.

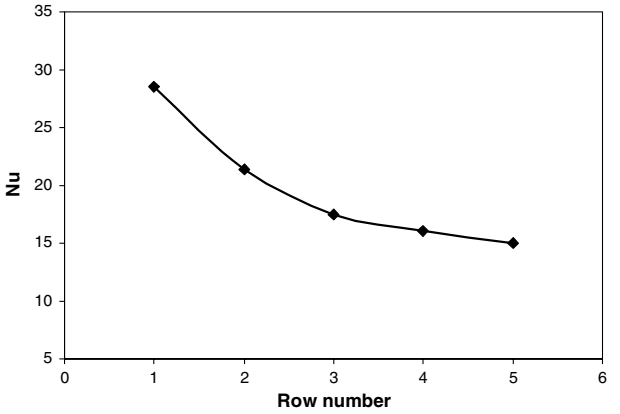

Fig. 6 Row-averaged Nusselt number distribution of heat sources ($Re = 495$).

B. Measured Temperature Profiles

In Fig. 4, a typical row-averaged temperature distribution in the flow direction for the five rows used is shown for $Re = 495$. It can be noted that heater temperatures continuously increase in the main flow direction with the row number. This behavior is also true for the other Reynolds numbers, as illustrated in Fig. 5. This trend of the temperature rise, which can be attributed to the thermal-wake effect of each block on the other blocks, agrees well with the previous studies [25,26].

For the free-convection condition, the surface temperature is maximal at the middle of the board. Indeed, from the measured data plotted in Fig. 5, it is shown that the modules in the middle column were found to have higher temperature values relative to the other two columns. The hottest module was the module in the middle of the board. This is mainly due to the heat accumulated at the center of the circuit board. The position of the maximum surface temperature tends to change toward the direction of the exit as the air velocity increases. Overall, increasing the Reynolds number results in a decrease of the electronic module temperature.

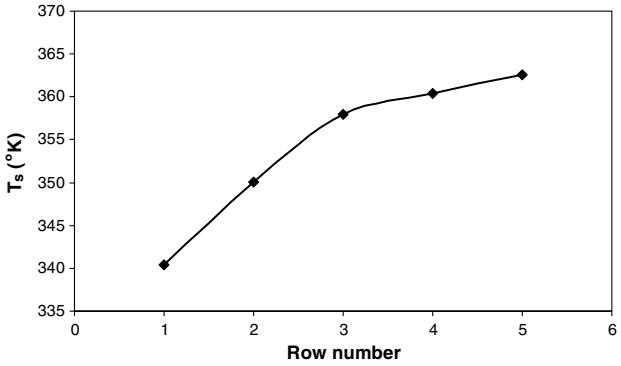

Fig. 4 Row-averaged temperature distributions of heat sources ($Re = 495$).

C. Nusselt Numbers

Figures 6 and 7 have been prepared similarly to Figs. 4 and 5 in order to show the variation of Nusselt number with row number for different Reynolds numbers. Variations in these figures show typical forced-convective flow characteristics for all Reynolds numbers.

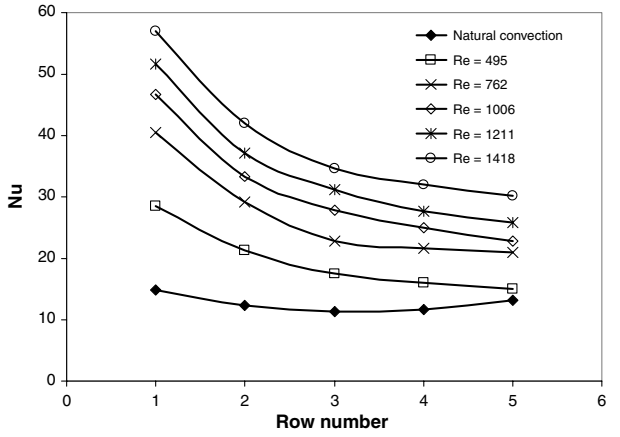

Fig. 7 Variation of Nusselt number with row number for different Reynolds numbers.

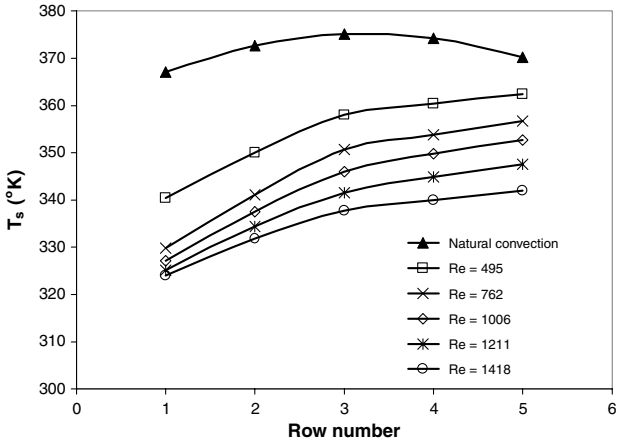

Fig. 5 Effect of Reynolds number on the row-averaged heat-source temperature.

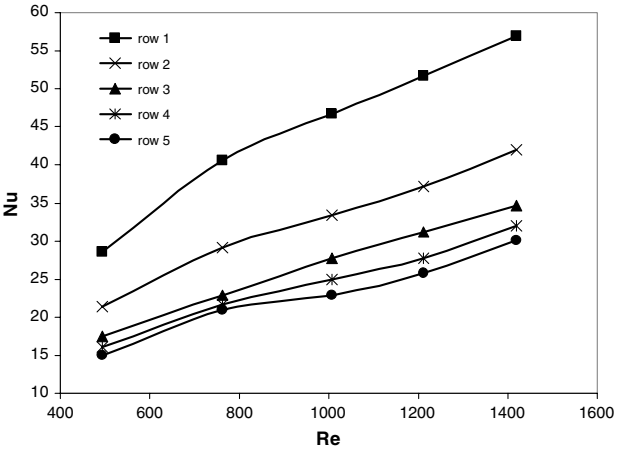

Fig. 8 Variation of Nusselt number with Reynolds numbers for all five rows.

In addition, the Nusselt number increases as the Reynolds number increases and it decreases as the distance of the heat source from the jet increases (Fig. 7). This can be attributed to the increase of the spent flow velocity with the increase of Reynolds number, which leads to high heat removal rate and, in consequence, high Nusselt number. This trend of the Nusselt number agrees well with previous studies [27–29] for cooling of inline array blocks by parallel flows, which showed the increase of the heat transfer coefficient of a block with both the decrease of its distance from the entrance and the increase of the air Reynolds number. Also, the first two rows show the largest differences between the different Reynolds numbers, where large Reynolds numbers produce larger Nusselt numbers at the beginning of the heated section. These differences start to diminish from the third row onward. The latter can be explained by the fact that the reduction in the Nusselt number due to forced-convection effects is balanced by an increase due to the buoyancy-driven secondary flow.

To more clearly understand the physical mechanisms involved in the heat transfer from the electronic modules under various operating conditions, the effects of the Reynolds number on the Nusselt number are drawn in Fig. 8 for all five rows individually. It is interesting to see how the effect of an increase of Reynolds number changes according to the row number. Nusselt number values for rows 1–3 exhibit a significant increase with increasing Reynolds number. This is due to the forced-convection nature of the heat transfer in that region. In contrast, the values for rows 4–5 show a slight increase. Furthermore, the first two rows show the largest differences between the Nusselt numbers. These differences diminish dramatically from the third row onward, confirming the information provided in Fig. 7.

D. Thermal-Wake Effect

The overall thermal-wake-generation correlation for different Reynolds numbers is shown in Fig. 9. The thermal-wake generation was found to be increasing at a high constant rate up to the middle of the board, then the rate decreases and remains almost constant up to the end of the board, regardless of the value of the Reynolds number. This shows that the dimensionless temperature is independent of heater location at different Reynolds numbers. However, when the heater is located adjacent to the inlet, lower component temperatures are seen at all Reynolds numbers, as a consequence of the entrance effect. It can also be seen in Fig. 9 that an increase in the Reynolds number results in a decrease in the dimensionless component temperature. This trend agrees with the results of Molki et al. [30], who showed that θ very slightly decreases with increasing Reynolds number in the case of cooling of inline array by parallel flow. The present trend of θ is also consistent with the results obtained by Turkoglu and Yucel [31] for cooling of a discrete heat source located on the left wall of an open-ended vertical channel.

It can generally be stated that the thermal-wake-generation function increases at the downstream region. Comparing the thermal-wake-generation correlation for each case, we can notice that the thermal system has its highest thermal-wake effect when the

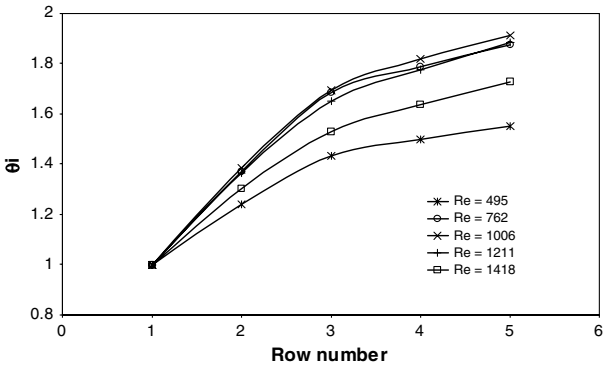

Fig. 9 Thermal-wake-generation function.

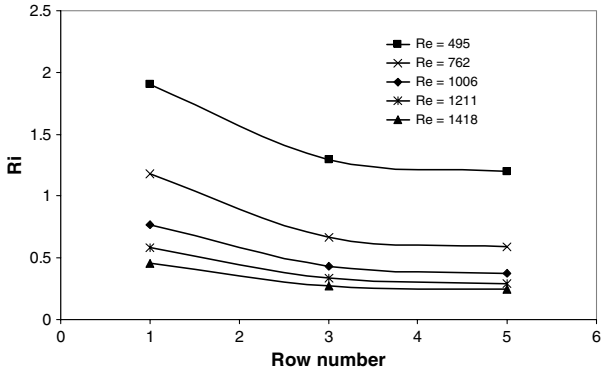

Fig. 10 Effect of buoyancy force as Reynolds number increases.

Reynolds number equals 1006 and has the lowest value when the Reynolds number equals 495.

The effect of buoyancy forces in mixed-convection flow can be shown by the plot of Richardson numbers shown in Fig. 10. The influence of buoyancy forces can be expected to decrease at the same position as the Reynolds number increase. It is considered to be of strong effect at values of Richardson numbers greater than unity and of small effect at values of Richardson numbers less than unity.

E. CFD Results

This section first reviews the results of the modeling and then compares them to the experimental data. Figure 11 shows the temperature distribution on the surface of the electronic board and

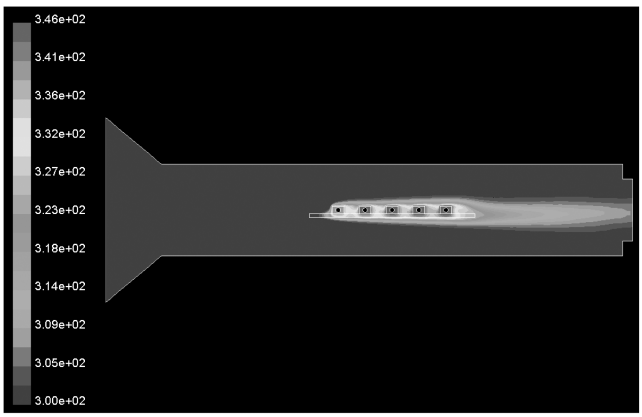

Fig. 11 Temperature distribution contour lines for the electronic board.

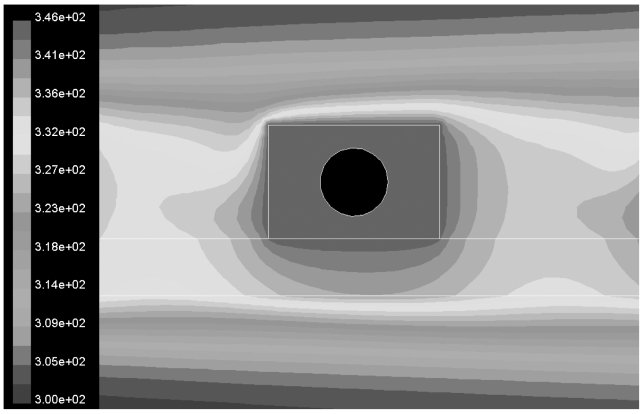

Fig. 12 Temperature distribution contour lines for modules in the third row.

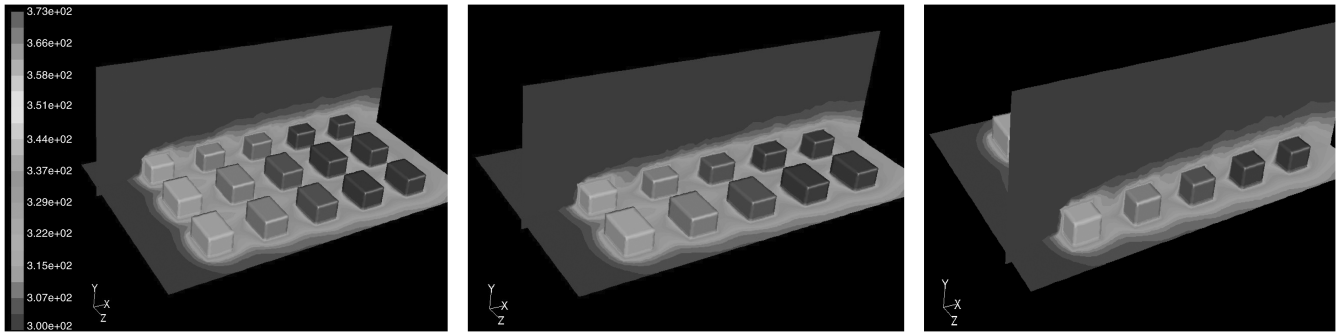

Fig. 13 Effect of additional obstructions on the surface temperature distribution.

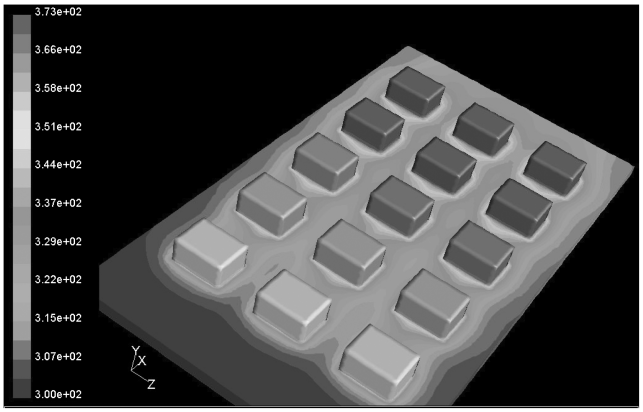

Fig. 14 Three-dimensional temperature distribution contours over modules' surfaces.

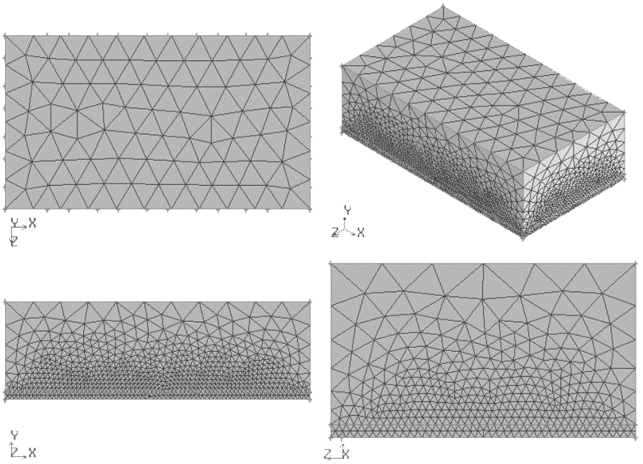

Fig. 15 Three-dimensional unstructured mesh.

the local ambient environment. The temperature values were found to be higher at the bottom of the module and to decrease gradually to the top, where the modules are exposed to fresh, cooler, air. This may suggest the application of a thermal heat sink on the bottom side to improve heat dissipation from the electronic board. Figure 12 shows the temperature distribution on the surface and within the vicinity of one module.

To improve the temperature distribution inside this region, one may need to enhance the flow turbulence. This will result on a heavy mixing process, leading to a tremendous improvement of the air convective heat transfer. One way of achieving this suggested solution is by introducing additional obstructions to the board. This will deflect the flow direction, which will result in higher mixing and thus better surface temperature distribution, as shown in Fig. 13.

The three-dimensional temperature distributions are shown on Fig. 14. It can be seen that the modules located away from the flow inlet are hotter relative to those located near the inlet.

In general, heaters in the same row will have the same temperature, due to weak velocity in the horizontal direction. Even though the temperature distribution given in Fig. 14 is not exactly symmetrical spanwise, the maximum temperature variation between the three modules in each row, as shown in Table 1, is very small (less than 0.6%). This is mainly caused by the unstructured mesh that had been used due to the geometry complexity of the model. It can be seen in Fig. 15 that the central modules have better grid refinement than the modules closer to the wall, hence the slight difference in temperatures between the modules of the same row.

Table 1 Maximum temperature variation in each row

Row	Temperature			Maximum variation, %
	m_1 wall	m_2 center	m_3 wall	
1	352.6	351.8	352.3	0.22
2	360.4	361.5	361.5	0.3
3	366.6	367.1	365.1	0.14
4	370.5	371.5	369.5	0.54
5	370.7	372.9	370.6	0.62

The simulation results were compared with the measured experimental results for validation. Figure 16 shows the average experimental module temperature compared with the simulated CFD temperature. It reveals that the thermal-wake generation of the simulated model is less significant when compared with the experimental results. Lower values of Reynolds number were found to coincide with better estimates at locations nearer the inlet. Larger values of Reynolds number were accompanied with better estimates of surface temperature at downstream regions.

The estimated values of the surface temperature were found to be of good agreement with the actual measured values. The maximum percentage error was found to be 4.9%, with a maximum standard deviation of 2.5 when considering different Reynolds number for the entire plate and of 1.7 when considering the local error variations at same locations. The error in the estimated values was found to be related to the values of the Reynolds numbers and the axial position on the board. Figure 17 shows the variation of the percentage-error values as Reynolds number increases.

One of the interesting observations is the mode of change of the position at which the software exactly estimated the measured value of surface temperature. This position was noted to change axially toward the downstream direction as Reynolds number increases. This phenomenon is illustrated on Fig. 18. In addition, the module surface temperatures were estimated exactly by the software, as the measured experimental values were found to be approximately equal to the average board temperature.

Studying Fig. 10 together with Fig. 18 reveals that the positions at which the software estimated accurate temperature values were the positions at which the buoyancy effect is of the same order as the momentum forces of the flow.

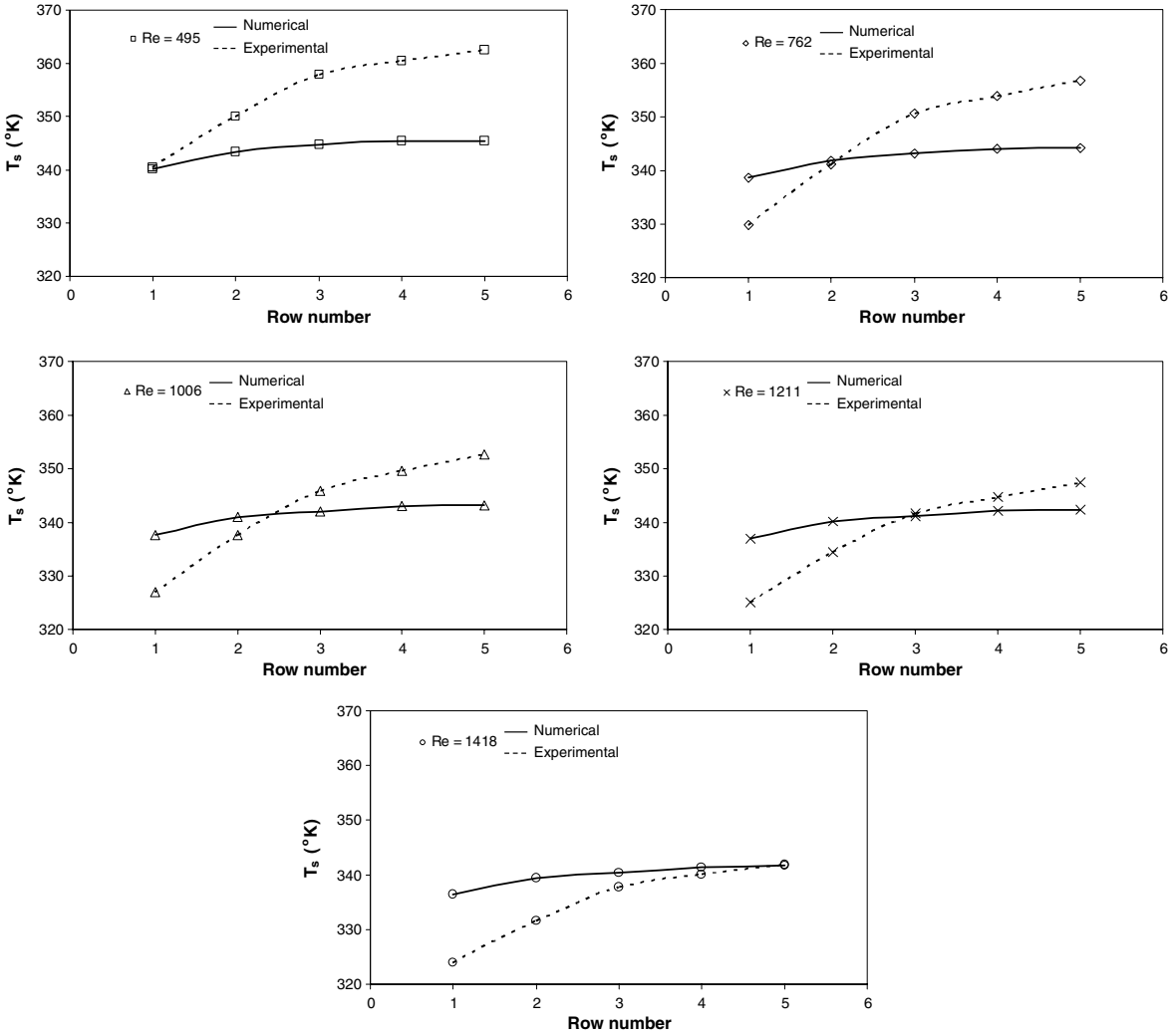

Fig. 16 Comparison between the experimental and numerical surface temperature for different Reynolds numbers.

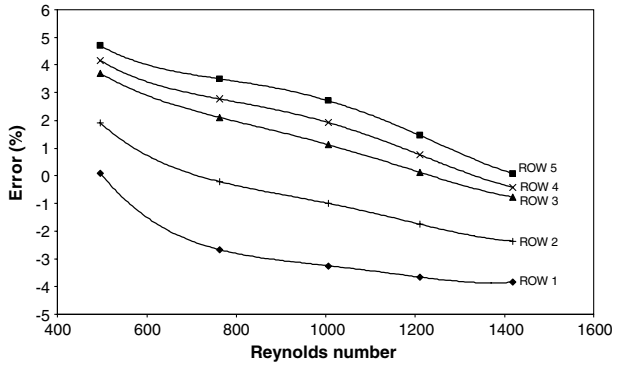

Fig. 17 Variation of the percentage error with Reynolds number.

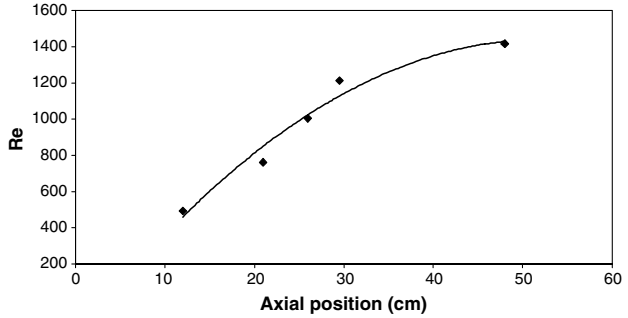

Fig. 18 Axial positions at which the software estimated exactly the measured surface temperatures at various Reynolds numbers.

V. Conclusions

Heat transfer from discrete heat sources in a simulated electronic circuit board under mixed-convection conditions has been investigated experimentally inside a horizontal rectangular channel and has been investigated numerically using FLUENT CFD software.

The values of the Reynolds number, at which the software exactly estimated the measured values, were found to be increasing following the trend of thermal-wake generation. This phenomenon may be related partially to the instability of the thermal boundary layer when the thermal wake exceeds a certain value with respect to different Reynolds numbers.

The agreement of the CFD software predictions was found to be very good when the buoyancy forces and the momentum forces are of the same order. A correction factor is needed to improve the CFD estimates at other conditions. The maximum percentage error was found to be 4.9%. The local surface temperatures, at which the software was able to predict the measured values, were always found to be very close to the mean temperature of the board.

The obtained results from this work provide valuable information for the thermal design of electronic packages. Components with the greatest power dissipation should be placed on the first and last rows, and those having low power dissipation should be placed in the middle rows. Moreover, the heat transfer enhancement was found to be largest for low Reynolds numbers, suggesting that heat transfer may be enhanced due to buoyancy induced flow by reducing the flow rate and, consequently, the ventilation power requirements for electronic packages.

Acknowledgments

The authors would like to thank International Islamic University Malaysia for funding this project. The authors would like also to thank M. F. Ismail and H. F. Bachok for their assistance in fabricating the experimental setup and running the computational fluid dynamics simulation and Lynn Mason for her help in editing this paper.

References

[1] Remsburg, R., *Advanced Thermal Design of Electronic Equipment*, International Thomson Publishing, Singapore, 1998.

[2] Bar-Cohen, A., and Kraus, A. D., *Advances In Thermal Modeling of Electronic Components and Systems*, Vol. 2, ASME Press, New York, 1990, pp. 41–107.

[3] Jeevan, K., Quadir, G. A., Seetharamu, K. N., and Azid, I. A., "Thermal Management of Multi-Chip Module and Printed Circuit Board Using FEM and Genetic Algorithms," *Microelectronics International*, Vol. 22, No. 3, 2005, pp. 3–15. doi:10.1108/13565360510610486

[4] Kandasamy, R., and Subramanyam, S., "Application of Computational Fluid Dynamics Simulation Tools for Thermal Characterization of Electronic Packages," *International Journal of Numerical Methods for Heat and Fluid Flow*, Vol. 15, No. 1, 2005, pp. 61–72. doi:10.1108/09615530510571958

[5] Sathe, S., and Sammakia, B., "A Review of Recent Development in Some Practical Aspects of Air-Cooled Electronic Packages," *Journal of Heat Transfer*, Vol. 120, No. 4, 1998, pp. 830–839. doi:10.1115/1.2825902

[6] Begles, A. E., "Evolution of Cooling Technology for Electrical, Electronic and Microelectronic Equipment," *IEEE Transactions on Components and Packaging Technologies*, Vol. 26, No. 1, 2003, pp. 6–15. doi:10.1109/TCAPT.2003.809664

[7] Saini, M., and Webb, R. L., "Heat Rejection Limits of Air-Cooled Plane Fin Heat Sinks for Computer Cooling," *IEEE Transactions on Components and Packaging Technologies*, Vol. 26, No. 1, 2003, pp. 71–79. doi:10.1109/TCAPT.2003.811465

[8] Bhattacharya, A., and Mahajan, R. L., "Finned Metal Foam Heat Sinks for Electronics Cooling in Forced Convection," *Journal of Electronic Packaging*, Vol. 124, No. 3, 2002, pp. 155–163. doi:10.1115/1.1464877

[9] Bar-Cohen, A., "State of the Art and Trends in the Thermal Packaging of Electronic Equipment," *Journal of Electronic Packaging*, Vol. 114, No. 3, 1992, pp. 257–270. doi:10.1115/1.2905450

[10] Bar-Cohen, A., "Thermal Management of Air- and Liquid-Cooled Multichip Modules," *IEEE Transactions on Components, Hybrids, and Manufacturing Technology*, Vol. 10, No. 2, June 1987, pp. 159–175. doi:10.1109/TCHMT.1987.1134734

[11] Bar-Cohen, A., and Krueger, W. B., "Thermal Characterization of Chip Packages: Evolutionary Development of Compact Models," *IEEE Transactions on Components and Packaging Technologies*, Vol. 20, No. 4, 1997, pp. 399–410. doi:10.1109/95.650929

[12] Kennedy, K. J., and Zebib, A., "Combined Free And Forced Convection Between Horizontal Parallel Plates: Some Case Studies," *International Journal of Heat and Mass Transfer*, Vol. 26, No. 3, American Society of Mechanical Engineers, New York, 1983, pp. 471–474. doi:10.1016/0017-9310(83)90052-2

[13] Kang, B. H., Jaluria, Y., and Tewari, S. S., "Mixed Convection Air Cooling of an Isolated Rectangular Heat Sources Module on a Horizontal Plate," *Proceedings of the 1988 ASME National Heat Transfer Conf.*, Vol. 2, American Society of Mechanical Engineers, New York, 1988, pp. 59–66.

[14] Huang, C. C., and Lin, T. F., "Buoyancy Induced Flow Transition Mixed Convective Flow of Air Through a Bottom Heated Horizontal Rectangular Duct," *International Journal of Heat and Mass Transfer*, Vol. 37, No. 8, 1994, pp. 1235–1255. doi:10.1016/0017-9310(94)90209-7

[15] Kerki, K. C., Sathyamurthy, P. S., and Patankar, S. V., "Laminar Mixed Convection in a Horizontal Semicircular Duct with Axial Nonuniform Thermal Boundary Condition on the Flat Wall," *Numerical Heat Transfer, Part A, Applications*, Vol. 25, No. 2, 1994, pp. 171–189. doi:10.1080/10407789408955943

[16] Leung, C. W., and Kang, H. J., "Convective Heat from Simulated Air-Cooled Printed-Circuit Board Assembly on Horizontal or Vertical Orientation," *International Communications in Heat and Mass Transfer*, Vol. 25, No. 1, 1998, pp. 67–80. doi:10.1016/S0735-1933(97)00138-3

[17] Chin, S., Liu, Y., Chan, S. F., Leung, C. W., and Chan, T. L., "Experimental Study of Optimum Spacing Problem in the Cooling of Simulated Electronic Package," *Heat and Mass Transfer*, Vol. 37, Nos. 2–3, 2001, pp. 251–257. doi:10.1007/s002310000168

[18] Jubran, B. A., and AL-Salaymeh, A. S., "Heat Transfer Enhancement in Electronic Modules Using Ribs and Film-Cooling-Like Techniques," *International Journal of Heat and Fluid Flow*, Vol. 17, 1996, pp. 148–154. doi:10.1016/0142-727X(95)00098-B

[19] Choi, C. Y., and Kim, S. J., "Conjugate Mixed Convection in a Channel: Modified Five-Percent Rule," *International Journal of Heat and Mass Transfer*, Vol. 39, No. 6, 1996, pp. 1223–1234. doi:10.1016/0017-9310(95)00195-6

[20] Holman, J. P., *Experimental Methods for Engineers*, McGraw–Hill, New York, 2001.

[21] Kline, S. J., and McClintock, F. A., "Describing Uncertainty in Single Sample Experiments," *Mechanical Engineering*, Vol. 75, 1953, pp. 3–8.

[22] Moffat, R. J., "Describing the Uncertainties in Experimental Results," *Experimental Thermal and Fluid Science*, Vol. 1, No. 1, 1988, pp. 3–17. doi:10.1016/0894-1777(88)90043-X

[23] Choi, M., and Cho, K., "Effect of the Aspect Ratio of Rectangular Channels on the Heat Transfer and Hydrodynamics of Paraffin Slurry Flow," *International Journal of Heat and Mass Transfer*, Vol. 44, No. 1, 2001, pp. 55–61. doi:10.1016/S0017-9310(00)00095-8

[24] Anderson, A. M., "A Comparison of Computational and Experimental Results for Flow and Heat Transfer from an Array of Heated Blocks," *Journal of Electronic Packaging*, Vol. 119, No. 1, 1997, pp. 32–39. doi:10.1115/1.2792198

[25] Huzayyin, A. S., Nada, S. A., Rady, M. A., and Faris, A., "Cooling an Array of Multiple Heat Sources by a Row of Slot Air Jets," *International Journal of Heat and Mass Transfer*, Vol. 49, Nos. 15–16, 2006, pp. 2597–2609. doi:10.1016/j.ijheatmasstransfer.2005.10.048

[26] Baskaya, S., Erturhan, U., and Sivrioglu, M., "Experimental Investigation of Mixed Convection from an Array of Discrete Heat Sources at the Bottom of a Horizontal Channel," *Heat and Mass Transfer*, Vol. 42, No. 1, 2005, pp. 56–63. doi:10.1007/s00231-005-0658-1

[27] Moffat, R. J., Arvizu, D. E., and Ortega, A., "Cooling Electronic Components: Forced Convection Experiments with an Air Cooled Array," *Heat Transfer in Electronic Equipment*, Vol. 48, American Society of Mechanical Engineers, Heat Transfer Div., New York, 1985, pp. 17–27.

[28] Moffat, R. J., and Anderson, A. M., "Applying Heat Transfer Coefficient Data to Electronic Cooling," *Journal of Heat Transfer*, Vol. 112, No. 4, 1990, pp. 882–890. doi:10.1115/1.2910495

[29] Azar, K., and Moffat, R. J., "Evaluation of Different Heat Transfer Coefficient Definitions," *Electronics Cooling*, Vol. 1, No. 1, 1995, pp. 21–23.

[30] Molki, M., Faghri, M., and Ozbay, O., "A Correlation for Heat Transfer and Wake Effect in the Entrance Region of an Inline Array of Rectangular Blocks Simulating Electronic Components," *Journal of Heat Transfer*, Vol. 117, No. 1, 1995, pp. 40–46. doi:10.1115/1.2822320

[31] Turkoglu, H., and Yucel, N., "Mixed Convection in Vertical Channels with a Discrete Heat Source," *Heat and Mass Transfer*, Vol. 30, No. 3, 1995, pp. 159–166. doi:10.1007/BF01476525